31.3 A Rectifier-less Piezoelectric Energy-Harvesting Interface with a Sense & Track MPPT Achieving Single-Cycle Convergence and 568% Shock Power Improvement

Shunmin Jiang*[1], Xinling Yue*[1], Yuchen Ma[1], Chao Wang[2], Sijun Du[1]

[1]Delft University of Technology, Delft, The Netherlands
[2]Huazhong University of Science and Technology, Wuhan, China

*Equally Credited Authors (ECAs)

The number of edge sensors for the Internet-of-Things (IoT) has been increasing dramatically every year to feed servers and artificial intelligence (AI) with more and more data. While powering these edge devices with batteries becomes unrealistic, piezoelectric energy harvesting (PEH) provides a promising power solution when they are implemented in industry, machines, and infrastructures. In these application scenarios, there are two main types of kinetic energy: periodical vibrations with stable amplitudes and shocks with varying amplitudes. While most reported bias-flip rectifiers and associated maximum power point tracking (MPPT) techniques perform well under periodical vibration inputs [1–4] compared to other architectures [5–10], their performance decays sharply under shock conditions due to the insufficient impedance-matching speed to accommodate fast varying input amplitude [11]. To efficiently harvest energy from real-world environments where both periodical and shock excitations exist, this paper proposes a rectifier-less interface with a sense & track (S&T) MPPT algorithm, which converges to a new maximum power point (MPP) in only one vibration cycle. This allows the PEH system to efficiently harvest kinetic energy from any form of vibrations with large and fast input amplitude variations.

Various maximum power point tracking (MPPT) techniques (Fig. 31.3.1 top) were proposed in previous works, including fractional open-circuit voltage (FOCV), perturb & observe (P&O) and duty-cycle-based (DCB) algorithms. The FOCV algorithm intermittently samples the PT's open-circuit voltage amplitude (V_{OC}) and regulates the output voltage V_{RECT} to the MPP, $V_{MPP}=V_{OC}/(1-\eta_F)$, where η_F is the voltage flipping efficiency [12]. Despite its simplicity and the fast determination of target V_{MPP}, the energy wastage during V_{OC} sampling and delayed (non-continuous) tracking limits its performance, especially during shock inputs when the MPP changes every cycle. The P&O and DCB algorithms [13–17] are closed-loop control techniques, monitoring output power and the rectifier's cut-off duty cycle, respectively, to adjust V_{RECT} step by step towards the V_{MPP}. Though they can achieve continuous and robust MPPT, convergence speed is severely limited due to the unknown target V_{MPP}. Hence, many vibration cycles are usually needed to reach the new V_{MPP}, making them unsuitable for shock excitations [15–17].

In the proposed S&T MPPT algorithm, the FOCV and DCB MPPT algorithms are hybridized in a way that their inherent drawbacks (FOCV: V_{OC}-sampling energy waste and non-continuous; DCB: slow convergence) are eliminated, while their advantages (FOCV: fast new V_{MPP} determination; DCB: continuous sensing) are kept. As shown in Fig. 31.3.1(bottom left), a piezoelectric transducer (PT) can be modeled as an AC source, I_P, in parallel with C_P and R_P. It can be observed that the voltage across the PT, V_{PT}, increases by a V_{OC} when it is cut off from the rectifier for T/4, where T is the vibration period. Hence, this principle can be used for continuous V_{OC} sampling without cutting off the PT from the circuit for a full period to measure the V_{OC}. The sampled V_{OC} will be used to calculate the V_{MPP} for the next half cycle. Figure 31.3.1 bottom-right explains the principle for V_{OC}-decreasing and V_{OC}-increasing cases. There are two interleaved phases, "sense" and "track", performing V_{OC}-sensing and MPP tracking, respectively. In the "sense" half cycle, the rectifier's cut-off duty cycle is fixed at 50%, so the voltage increase in V_{PT} equals V_{OC} and it is sampled. Then, the system calculates the next V_{MPP} while V_{PT} is regulated at the current voltage level with multi-shot energy transfer from C_P to C_S. After the bias-flip, the "track" phase comes. The new V_{MPP} is known, and it is where V_{PT} needs to be regulated. In the case of a decreasing V_{OC}, the cut-off duty cycle in the "track" phase is less than 50%; in the reversed case, it is higher than 50%. In periodical vibrations with stable V_{OC}, the cut-off duty cycle in "track" keeps at 50%. Compared with three conventional MPPT algorithms, the proposed achieves single-cycle V_{MPP} determination and continuous MPPT (advantages of FOCV and DCB). Besides, it does not introduce open-circuit energy loss (drawback of FOCV).

Power stage operations are shown in the upper part of Fig. 31.3.2. The power stage consists of a PT, an off-chip inductor L, an off-chip storage capacitor C_S, and eight on-chip power switches. Φ_P and Φ_N are symmetrical, decided by the polarity of V_{PT}. Taking positive-V_{PT} (Φ_P) as an example, in Φ_{1P}, S_P is closed and C_P is charged with harvested energy. When V_{PT} reaches the setting V_{Reg}, DC-DC is activated. During the regulation Φ_{2P}, S_P, S_{AP}, and S_{LN} are closed in a short pulse and energy is transferred from C_P to L. Then S_{LP} and S_{BP} are closed in the followed Φ_{3P}, to discharge L, charging the storage component. Φ_{2P} and Φ_{3P} repeat many times during a half cycle to maintain V_{PT} around V_{Reg}. When the bias-flip moment arrives, the circuit enters Φ_4, S_{AP}, and S_{AN} are closed, forming an LC-tank to flip V_{PT}. With a rectifier-less structure, DC-DC regulation plays an important role in the whole MPPT algorithm flow, which is shown in the bottom left. In the start-up stage, the system uses one cycle to rapidly build up V_{PT} and measure the periods. Then the system enters the sampling half-cycle. Once build-up time reaches T/4 (50% duty cycle), V_{OC} is sampled and V_{MPP} is calculated with the equation $V_{MPP}=V_{OC}/(1-\eta_F)$, where the factor $1/(1-\eta_F)$ is calculated from bias-flipping voltage. After DC-DC regulation, the tracking half-cycle arrives. I_P would charge C_P to V_{MPP}. Then, the next circulation starts. The system architecture is shown in Fig. 31.3.2 bottom right, which consists of a power stage, an MPP monitor module (including V_{OC} Sampler, Duty Cycle Detector, and V_{MPP} Generation), DC-DC Controller, switch drivers, and level shifters. V_{PT} is sensed to determine the P/N phase and to calculate V_{MPP}, which is executed by the MPP Monitor. V_{MPP} is sent into the DC-DC voltage arbiter. At the same time, CYC_S and CYC_T are produced by the Duty Cycle Detector block to indicate it is in the "sense" or "track" phase. CYC_S and CYC_T will control the DC-DC Voltage Arbiter to choose V_{Reg} from V_{50DC} and V_{MPP}, which are the voltage where V_{PT} needs to be regulated in "sense" and "track" phases, respectively. Finally, the switching signals will be generated to drive the power switches through level shifters.

The MPP monitor module is shown in Fig. 31.3.3. The module consists of four blocks. The Duty Cycle Detector determines the duty cycle of the build-up phase by utilizing a high output impedance current mirror to charge capacitors array with full range tunable duty cycle. Receiving the trigger signal from the duty cycle detector, the V_{OC} sampler senses 1/2 V_{OC} by charge division and the sampled signal connects to the negative node of the comparator. At the same time, a 5-bit binary capacitor array in the V_{MPP} Generation block will enter phase1, and currents with different weighed sizes will charge capacitors with the same value linearly, generating 2n-2×V_{CAP}. 0.5V_{CAP} is chosen to be the reference bit, once it's equal to 0.5V_{OC}, the MPP State Monitor would produce signals, making cap cells enter phase2. When all the cells are connected in series, the top end voltage is V_{MPP}. Before the next MPP circulation, the circuit will enter phase3 to clear the charge. The generating range is between 0.25V_{OC} and 7.75 V_{OC}, with a resolution of 0.25V_{OC}. Choosing the factor is based on the actual V_{PT} flipping efficiency according to the V_{MPP} equation.

The proposed circuit is fabricated in a 0.18μm BCD process and tested with a 142nF/219.4Hz piezoelectric transducer. Figure 31.3.4 top shows the waveforms when the PT is excited by shocks. Only when a certain V_{OC} is detected would the circuit wake up; otherwise, it stays in the sleep mode, as indicated by the *SLEEP* signal. The zoomed-in waveform is shown in the bottom left, in which the V_{PT} is constantly tracking the MPP. The shown single shock ends in 32 cycles, experiencing an attenuation from 4V to 0V. The start-up waveforms and stable MPPT process are shown in the bottom right. Figure 31.3.5 top shows the measured waveform when the PT is driven under periodical excitations, with the gradually increasing V_{OC} to show the MPPT. The output power versus V_S under the periodical and shock excitations is shown at the bottom. The power extraction enhancement compared to a full-bridge rectifier (FBR) in periodical and shock situations are 718% and 568%, respectively. The output power is weakly coupled to V_S in the suitable region (2~3V) thanks to the embedded MPPT.

Figure 31.3.6 shows the comparison table between the proposed circuit and the state-of-the-art works. Compared to traditional FOCV [12] techniques, the proposed MPPT algorithm can achieve continuous MPPT. Compared to P&O [15] and DCB [17] designs, a single-cycle MPPT convergence time is achieved and this is independent of the load capacitor size. The proposed system achieves high power improvement under shock excitations. Figure 31.3.7 shows the die micrograph of the fabricated chip that has an active area of 0.67mm^2.

2025 IEEE International Solid-State Circuits Conference (ISSCC) | 979-8-3315-4101-9/25/$31.00 ©2025 IEEE | DOI: 10.1109/ISSCC49661.2025.10904749

Authorized licensed use limited to: TU Delft Library. Downloaded on July 30,2026 at 13:38:41 UTC from IEEE Xplore. Restrictions apply.

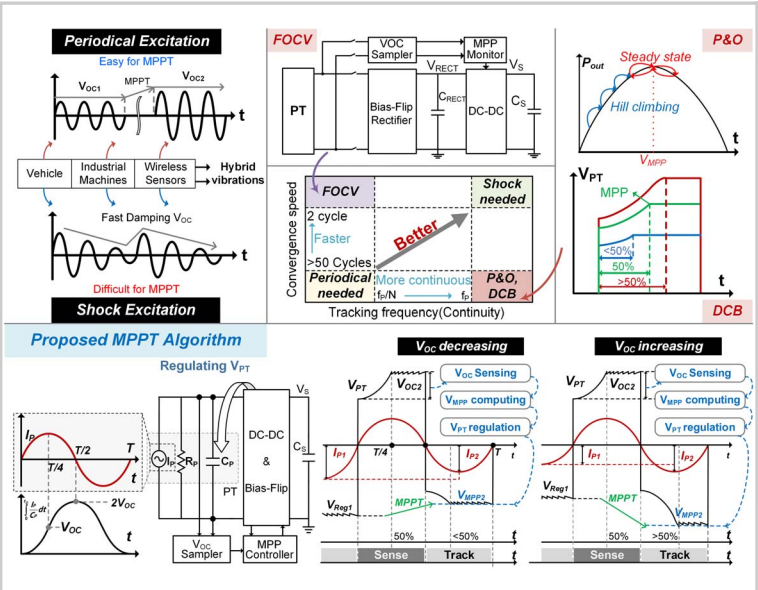


Figure 31.3.1: Conventional MPPT techniques and the principle of the proposed S&T MPPT architecture.

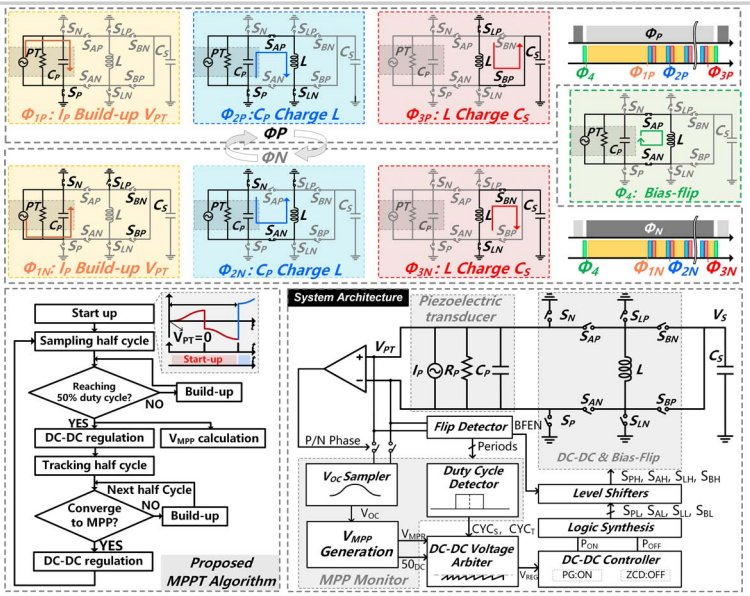


Figure 31.3.2: Principle of the proposed power stage circuit (top); S&T MPPT algorithm flow chart (bottom left) and circuit architecture (bottom right).

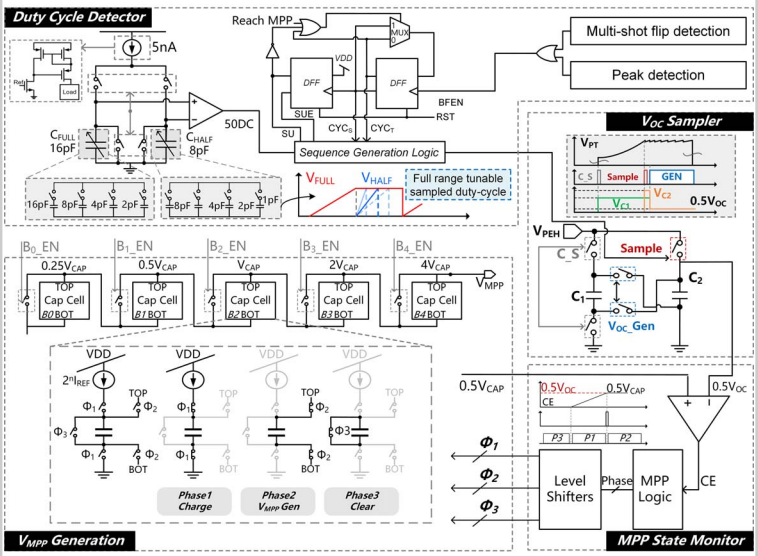


Figure 31.3.3: Implemented MPP Monitor block architecture (top) consisting of Duty-cycle Detector, V_{OC} Sampler, MPP State Monitor and V_{MPP} Generation sub-module.

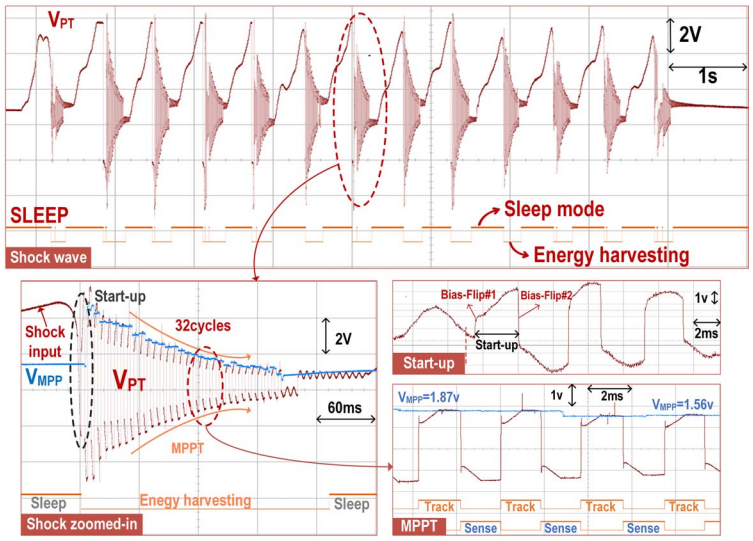


Figure 31.3.4: Waveform of V_{PT} under random shock excitation with 1~2 Hz excitation frequency(top); Zoom-in waveform of start-up phase and MPPT process (bottom).

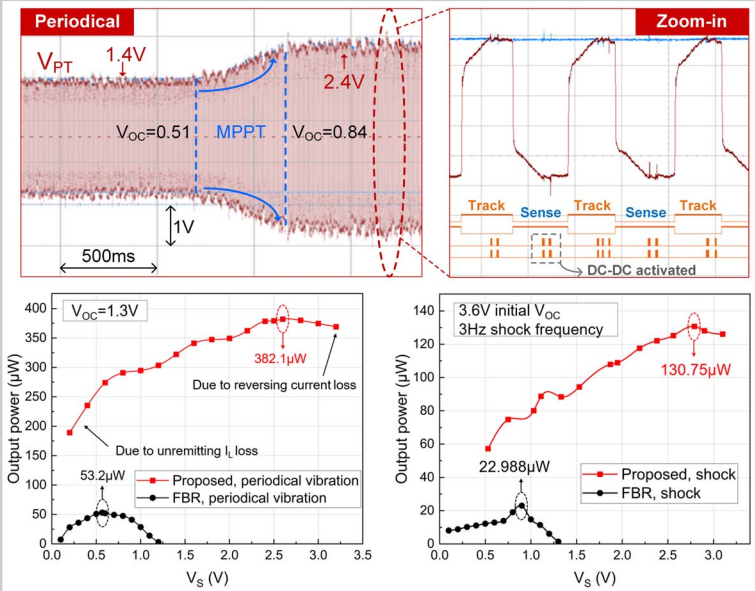


Figure 31.3.5: Periodical MPPT operation and zoon-in waveforms(top); The output power compared to FBR under periodical and shock excitations, respectively.

Parameters	This work	[12]ISSCC'14	[11]ISSCC'16	[10]JSSC'18	[15]ISSCC'20	[17]ISSCC'23
Rectifier Type	V_{PT} Regulation	FBR	SSHI	SECE	SECE	SSHI
Technology	0.18um	0.35um	0.35um	40nm	0.6um	0.18um
Piezoelectric capacitance	142nF	11nF	26/20/9nF	43nF	24nF	42nF
Resonant Frequency	219.4Hz	100Hz	134.6-229.2Hz	75.4	56Hz	230Hz
MPPT algorithm	S&T	FOCV	FOCV	N/R	P&O	DCB
MPP Convergence time	1 Cycle	*~10 Cycle	N/R	N/R	*~840 Cycle	*~180Cycle
Continuous MPP	Yes	NO	NO	Yes	Yes	Yes
AD/DA needed?	NO	NO	NO	NO	Yes	NO
Excitation type	Periodic & shock	Periodic	Periodic& shock	Periodic & shock	Periodic	Periodic
Power improvement	718%(Periodic) 568%(shock)	97%	681%(Periodic) 289%(Shock)	314%(Periodic) 420%(shock)	417%	738%

N/R : Not reported
* : Estimated

Figure 31.3.6: Comparison of the S&T MPPT interface circuit and state-of-the-art piezoelectric energy harvesting circuits.

Authorized licensed use limited to: TU Delft Library. Downloaded on July 30,2026 at 13:38:41 UTC from IEEE Xplore. Restrictions apply.

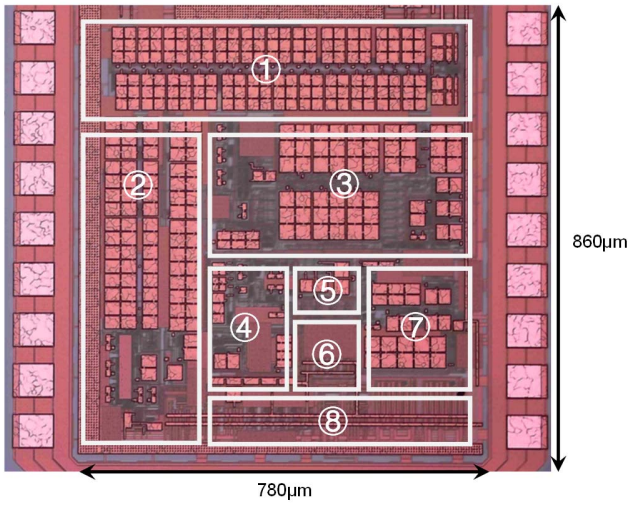


Figure 31.3.7: Die micrograph.

References:

[1] Y.K. Ramadass and A.P. Chandrakasan, "An Efficient Piezoelectric Energy Harvesting Interface Circuit Using a Bias-Flip Rectifier and Shared Inductor," *IEEE JSSC*, vol. 45, no. 1, pp. 189-204, Jan. 2010.

[2] S. Du and A.A. Seshia, "An Inductorless Bias-Flip Rectifier for Piezoelectric Energy Harvesting," *IEEE JSSC*, vol. 52, no. 10, pp. 2746-2757, Oct. 2017.

[3] Z. Chen et al., "Piezoelectric Energy-Harvesting Interface Using Split-Phase Flipping-Capacitor Rectifier With Capacitor Reuse for Input Power Adaptation," *IEEE JSSC*, vol. 55, no. 8, pp. 2106-2117, Aug. 2020.

[4] Y.-W. Jeong et al., "A Scalable N-Step Equal Split SSHI Piezoelectric Energy Harvesting Circuit Achieving 1170% Power Extraction Improvement and 22nA Quiescent Current with a 1μH–to–10μH Low-Q Inductor," *ISSCC*, pp. 438-439, Feb. 2023.

[5] G.K. Ottman et al., "Adaptive piezoelectric energy harvesting circuit for wireless remote power supply," *IEEE Transactions on Power Electronics*, vol. 17, no. 5, pp. 669-676, Sept. 2002.

[6] T.T. Le et al., "Piezoelectric micro-power generation interface circuits," *IEEE JSSC*, vol. 41, no. 6, pp. 1411-1420, June 2006.

[7] T. Hehn et al., "A Fully Autonomous Integrated Interface Circuit for Piezoelectric Harvesters," *IEEE JSSC*, vol. 47, no. 9, pp. 2185-2198, Sept. 2012.

[8] D. Kwon and G. A. Rincón-Mora, "A Single-Inductor 0.35 μm CMOS Energy-Investing Piezoelectric Harvester," *IEEE JSSC*, vol. 49, no. 10, pp. 2277-2291, Oct. 2014.

[9] Y. Peng et al., "An Efficient Piezoelectric Energy Harvesting Interface Circuit Using a Sense-and-Set Rectifier," *IEEE JSSC Circuits*, vol. 54, no. 12, pp. 3348-3361, Dec. 2019.

[10] A. Morel et al., "A Shock-Optimized SECE Integrated Circuit," *IEEE JSSC*, vol. 53, no. 12, pp. 3420-3433, Dec. 2018.

[11] D. A. Sanchez et al., "A 4μW-to-1mW Parallel-SSHI Rectifier for Piezoelectric Energy Harvesting of Periodic and Shock Excitations with Inductor Sharing, Cold Start-Up and Up to 681% Power Extraction Improvement," *ISSCC*, pp. 366-367, Feb. 2016.

[12] M. Shim et al., "Self-Powered 30 μW to 10 mW Piezoelectric Energy Harvesting System With 9.09 ms/V Maximum Power Point Tracking Time," *IEEE JSSC,* vol. 50, no. 10, pp. 2367-2379, Oct. 2015

[13] S. Li et al., "A Piezoelectric Energy-Harvesting System with Parallel-SSHI Rectifier and Integrated MPPT Achieving 417% Energy-Extraction Improvement and 97% Tracking Efficiency," *IEEE Symp. VLSI Circuits*, pp. 324-325, June 2019.

[14] Y. Cai and Y. Manoli, "A Piezoelectric Energy-Harvesting Interface Circuit with Fully Autonomous Conjugate Impedance Matching, 156% Extended Bandwidth, and 0.38μW Power Consumption," *ISSCC*, pp. 148-149, Feb 2018.

[15] A. Morel et al., "Self-Tunable Phase-Shifted SECE Piezoelectric Energy-Harvesting IC with a 30nW MPPT Achieving 446% Energy-Bandwidth Improvement and 94% Efficiency," *ISSCC,* pp. 488-489, Feb. 2020.

[16] C. Xie et al., "Fully Integrated Frequency-Tuning Switched-Capacitor Rectifier for Piezoelectric Energy Harvesting," *IEEE JSSC*, vol. 58, no. 8, pp. 2337-2348, Aug. 2023.

[17] X. Yue et al., "A Bias-Flip Rectifier with a Duty-Cycle-Based MPPT Algorithm for Piezoelectric Energy Harvesting with 98% Peak MPPT Efficiency and 738% Energy-Extraction Enhancement," *ISSCC*, pp. 442-443, Feb. 2023.

Authorized licensed use limited to: TU Delft Library. Downloaded on July 30,2026 at 13:38:41 UTC from IEEE Xplore. Restrictions apply.

979-8-3315-4101-9/25/$31.00 ©2025 IEEE